Ionizations of Liquid Water from Charged-cell Periodic Subsystem DFT and Embedded Coupled Cluster Simulations

Jessica Martinez[1], Pablo Ramos[1], Andre Gomes[2], Johannes Tölle[3], and Michele Pavanello*[1]

[1] *Department of Chemistry, Rutgers University, Newark, New Jersey*
[2] *Université de Lille, CNRS, UMR 8523 – PhLAM – Physique des Lasers, Atomes et Molécules, Lille, France*
[3] *Theoretische Organische Chemie, OrganischChemisches Institut and Center for Multiscale Theory and Computation (CMTC), Westfälische Wilhelms-Universität Münster, Corrensstraße 40, 48149, Münster, Germany*

* *Email: m.pavanello@rutgers.edu*

Abstract

Modeling the ionization potential (IP) and electron affinity (EA) of liquid water is challenging for two reasons: (1) the bulk-like nature of the liquid imposes the use of periodic boundary conditions (PBCs), which pose roadblocks when considering charge systems; (2) quantitative electronic structure methods, such as coupled cluster, are generally not available in PBCs. In this work, we tackle both challenges by employing subsystem DFT to split the extended system into a collection of finite subsystems embedded by extended, infinite subsystem. This is achieved by an impurity model [1] where high ab initio method as coupled cluster wavefunctions can be introduced to evaluate the water molecules' energy functionals.

The liquid's electronic structure is expressed in subsystem contributions by invoking nonadditive density functionals whereby the total energy of the liquid is expressed as the sum of molecule-additive and nonadditive contributions [2]. The inter-molecular interaction is split into Coulumb interactions, and such nonadditive terms as the noninteracting kinetic energy and the noninteracting exchange-correlation [2]. These contributions represent interactions related among others to exchange, van der Waals and Pauli repulsion and are all bifunctional of the subsystem densities [1].

The final IP/EA values reproduce the experimental values to within 0.5 eV and are determined averaging over two different systems of 64 and 256 water molecules (or subsystems) considered in the corresponding simulation cell, calculated by the energy difference of the neutral and the polarized system (Called SCF method) [3, 4].

1 Introduction

The high-accuracy calculations of ionization potentials (IPs) and electron affinities (EAs) of condensed-phase molecular systems as liquid water has represented a challege for the last years in both experimental and computational fields [1, 5–7]. Thus, ionized states of the electrons take part in many crucial processes in electrochemistry, photochemistry as well as peculiar states of matter as excess electrons solvated in liquid water [8]. The most recent theoretical report of IP and EA values [9] shows that using quasi-particle self-consistent GW calculations and implicit vertex correction in many-body perturbation (MBPT) remarkably affect the EA of liquid water previously reported [5] by Gaiduk et al by about 1eV. Therefore, they through self-consistent GW approach with an implicit vertex correction based on the projector augmented wave (PAW) method, which is the most accurate pseudo-potential [10] (PPs available), and combined with Bethe–Salpeter equation established values of 10.2 and 1.1 eV, for IP and EA of liquid water, respectively.

Following the trend and now including the use of periodic boundary conditions (PBC) another method was introduced [1] to determine the ionization potentials (IPs) and electron affinities (EAs) of liquid water. Based on determining successfully a quatum-mechanical model for charged species in PBC which is able to face the complications related to the long-ranged nature of the Coulomb Kernel $w(r, r^{'}) = \frac{1}{|r-r^{'}|}$, which decays to zero when two charges are far away in real space. Indeed, it was achieved using an impurity model with two remarkable qualities: 1) The charged periodic system is replaced by a non-periodic one which is still truly extended (ie., of infinite size) and 2) The potentials of the neutral and the charged system are pegged to a common reference.

The former requires an ad hoc mapping of the infinite system (periodic) onto finite number of finite subsystems (non-periodic subsystems) and an extended (infinite) subsystem, using a formally exact density embedding method, subsystem DFT [11]. Meanwhile, achieving the latter only requires finding a consistent choice for the $G = 0$ component of the Coulomb Kernel in

a reciprocal space. The use of the reciprocal space is only chosen for avoiding the complication of dealing with convergent integrals [12] In addition, in PBC the physical Coulomb kernel is only the one represented in a reciprocal space $w(G) = \frac{4\pi}{|G|^2}$ where $G \epsilon \mathbb{R}^3$. Even though, when $G = 0$ the Coulomb kernel becomes undefined the total charged density $\rho(G)$ is zero for $G = 0$, which is not problematic.

Here we present an update of the current state-of-the-art of liquid water IPs and EAs base on an impurity model using an exact density embedding method, subsystem DFT. This may allow us to contribute to the discussion generated about the most accurate value for the EAs of bulk water by using ab initio electronic structure [5, 8] by GW approximations. We begin with a brief theoretical framework description and follow on the description of the EAs and IPs of 64 and 256 bulk liquid water systems.

2 Theoretical Background

2.1 Mapping a periodic system into a collection of non-periodic subsystems and one periodic subsystem

To cast DFT in a subsystem fashion, we invoke nonadditive functionals in which each energy term of the supersystem is expressed as the sum of additive and nonadditive contributions [13]. Therefore, when dealing with a finite subsystem with electron density η_I, and an infinite or extended subsystem with electron density η - η_I, the total density can be defined as the sum of the finite subsystem and the extended subsystem, and the total energy is given by,

$$E_{tot} = E_{[}\eta_I] + E_{[}\eta - \eta_I] + E^{int}[\eta_I, \eta - \eta_I] \tag{1}$$

The interaction energy can be broken down into the following contributions,

$$E^{int} = E_H^{int} + V_e^{int} N + T_s^{nad} + E_{xc}^{nad} \tag{2}$$

The two Coulombic terms E_H^{int} and $V_e^{int} N$ are the electron-electron and electro-nuclear interactions, respectively. And the nonadditive terms T_s^{nad} and E_{xc}^{nad}, represent the noninteracting kinetic energy of the system and the noninteracting exchange-correlation functionals, respectively [2]. The two last terms represent interactions related among other to exchange, van der Waals and Pauli repulsion and are all bifunctional of the two subsystem densities.

2.2 Coulomb interaction energy determination

As the electron-nuclear interaction can be treated in an equivalent way that the Hartree terms of the interaction energy, with the definition of the latter, we can map the complete theoretical background. The Hartree interaction energy then is defined between finite and infinite electronic system by,

$$E_H^{int} = \int_{\mathbb{R}^3} dr \int_{\Omega} dr' \frac{1}{|r - r'|} [\eta(r) - \eta_I(r)] \eta_I(r') \tag{3}$$

The integral over dr' takes place only over a finite volume Ω, here represented by the simulation cell. Contrariwise, the integral in dr is carried out over the entire space, due to the density $\eta - \eta_I$ is extended.

To describe the periodic potential interaction with a finite charge, first, we define the finite potential (define by an overbar) as being the potential which uses η_I (the electron density of the finite subsystem), as,

$$\bar{v}[\eta_I](r) = \int_\Omega dr' \frac{1}{|r - r'|} \eta_I(r') \tag{4}$$

For equations (3) and (4) the integral over dr' is carried out only over a finite volume Ω (typically the simualtion cell) because we expect $\eta_I(r) = 0$ when $r \notin \Omega$.

Therefore, computing the potential generated by the periodic system and using that in the computation of the interaction energy E_{int}, which is defined as,

$$E_{int} = \int_\Omega dr[v[\eta](n) - \bar{v}[\eta_I](r)]\eta_I(r) \tag{5}$$

Where $v[\eta](n)$ is the full periodic potential. The potentials are evaluated separately, in which the finite potential is commonly solve in real space because η_I is often the electron density of a finite system.

To compare total energies from periodic calculations the Coulomb kernel needs to be correctly referenced. In this work particularly, it is achieved imposing the $G = 0$ value of the periodic Coulomb kernel to match the same limit of the Coulomb kernel of a reference system. Here we choose the finite system to be the reference system. Thus, we referenced the periodic potential of the extended subsystem $(\eta - \eta_I)$ to the corresponding $G = 0$ component in the the ionized and neutral systems.

2.3 Embedding Scheme for the Nonionized System

For the neutral system, the Coulomb interaction energy can be expressed as a potential that maps the interaction of an accurately infinitely extended environment onto and isolated subsystem I,

$$v^I_{emb}[\eta](r) = v[\eta](r) - \bar{v}[\eta_I](r) \tag{6}$$

Where $v[\eta](r)$ is the total Coulomb potential of the system and $\bar{v}[\eta_I](r)$ the potential of the isolated subsystem I. The latter was evaluated using the Martyna-Tuckerman method whereby density η_I is assumed to be isolated and not periodic [13]. The embedding potential for the neutral subsystem can also be calculated directly from equation 3.

2.4 Impurity Model for the Ionized system

To obtain the embedding potential of a charged subsystem, we consider the system to be composed of an ionized subsystem embedded in a nonionized environment. To assemble the appropriate embedding potential, first was evaluated a screening potential, $v^{screen}[\eta_I](r) = v[\eta_I](r) - \bar{v}[\eta_I](r)$, understood as the electrostic potential of the periodically repeating water molecules have on a single lattice site, achiving the removal of only one isolated subsystem. The later $\bar{v}[\eta_I](r)$ is evaluated by Martyna-Tuckerman method[13]. The embedding potential depends on three densities: η the total system, η_I the neutral subsystem, and $\eta_I^{'}$ the charged subsystem, and has the form,

$$v^I_{emb,imp}[\eta, \eta_I^{'}, \eta_I](r) = v[\eta, \eta_I^{'}, \eta_I](r) - \bar{v}[\eta_I^{'}](r) \tag{7}$$

with

$$v[\eta, \eta_I^{'}, \eta_I](r) = v[\eta](r) + \Delta v^{screen}[\eta_I, \eta_I^{'}](r) \tag{8}$$

where $\Delta v^{screen}[\eta_I, \eta_I^{'}](r) = v^{screen}[\eta_I](r) - v^{screen}[\eta_I^{'}](r)$, which replace the electrostatic environment given by periodic images of the ionized subsystem having charged density $\rho_I^{'}$ with the neutral charged density ρ_I of the nonionized subsystem.

3 Computational Section

Embedding potentials for ionized and nonionized systems were obtained with embedded Quantum ESPRESSO (eQE) [14] employing ultrasoft pseudopotentials from PSL pseudopotential library [15]. PBE exchange-correlation functional [16] was used to evaluate the additive and nonadditive contributions to the total energy, and revAPBEK [17] to the nonadditive Kinetic energy functional. Following previously benchmarking studies [18, 19] a total of 40 Ry and 400 Ry were set as the energy cutoffs for the plane wave expansions of the molecular orbitals and the charge density, respectively.

The ground state calculation of each subsystem with the corresponding neutral and polarized embedding potential was determined through ADF [20] software. We selected each water molecule to be one subsystem (i.e, 64 and 256 subsystem in total) according to the most beneficial error cancelation, previously determined [18, 21–24], between the nonadditive kinetic energy and the nonadditive exchange-correlation functionals employed.

To make use of the embedding potential (EP) for both neutral and charged systems (obtained by eQE) in the ADF ground-state calculations, the atom centered grid function of eQE was used. The above is based on an interpolating function which splines the EP onto a custom grid, which provided the correct real-space representation due to the uses of atom centered basis functions. The general integral has the form,

$$v_{emb}^{\mu v} = \langle \chi_\mu | v_{emb} | \chi_v \rangle \tag{9}$$

This will generate a Gaussian cube file containing the splined embedding potential[14].

A comparison among Density Functional Theory (DFT), using GGA (PBE) [16], Hybrid (B3LYP) [25], Double-Hybrid (B2KPLYP [26], B2NCPLYP [27], and REVDSDBLYP [28]), and Statistical average of orbital potentials(SOAP) model[29, 30], Møller–Plesset perturbation theory (MP2) [31] and Hartree–Fock (HF) [32] level of theory was made, with the basis QZ4P. The final IP/EA values are calculated using an average for each of the 64 and 256 water molecules or subsystems considered in the simulation cell, calculated by the energy difference of the neutral and the polarized system (Called ΔSCF method) [3, 4].

4 Results

4.1 IPs of Bulk water

Using a random method a snapshot from an ab initio molecular dynamics (MD) based on subsystem DFT was selected base on a previous study [18]. We used that single snapshot which consists of a total of 64 subsystems (ie. 64 water molecules in a cubic box (a = 12.43 $\mathring{A}$) to compute the vertical IPs reproducing the density of the liquid.

The IPs and EAs were calculated in two ways: Isolated, each subsystem was computed independently and treated using MT assume isolated method [13], all the molecular geometries were taken from the MD. Embedded: we employed the impurity model above described by equation (7) and calculated the interaction energy following equation (5). The coulomb kernel of the $\eta - \eta_I$ extended neutral system, was taken as a reference because of their similarity between the neutral and ionized states, Figure 1.

We divided the succeeding analysis into three crucial parts. A complete comparison between previous eQE results for the IPs of bulk water with ADF calculation using the same functional PBE. Followed by the description among different previously mentioned DFT functionals. Closing with the comparison between HF with MP2 and MP2 with DFT functional methods

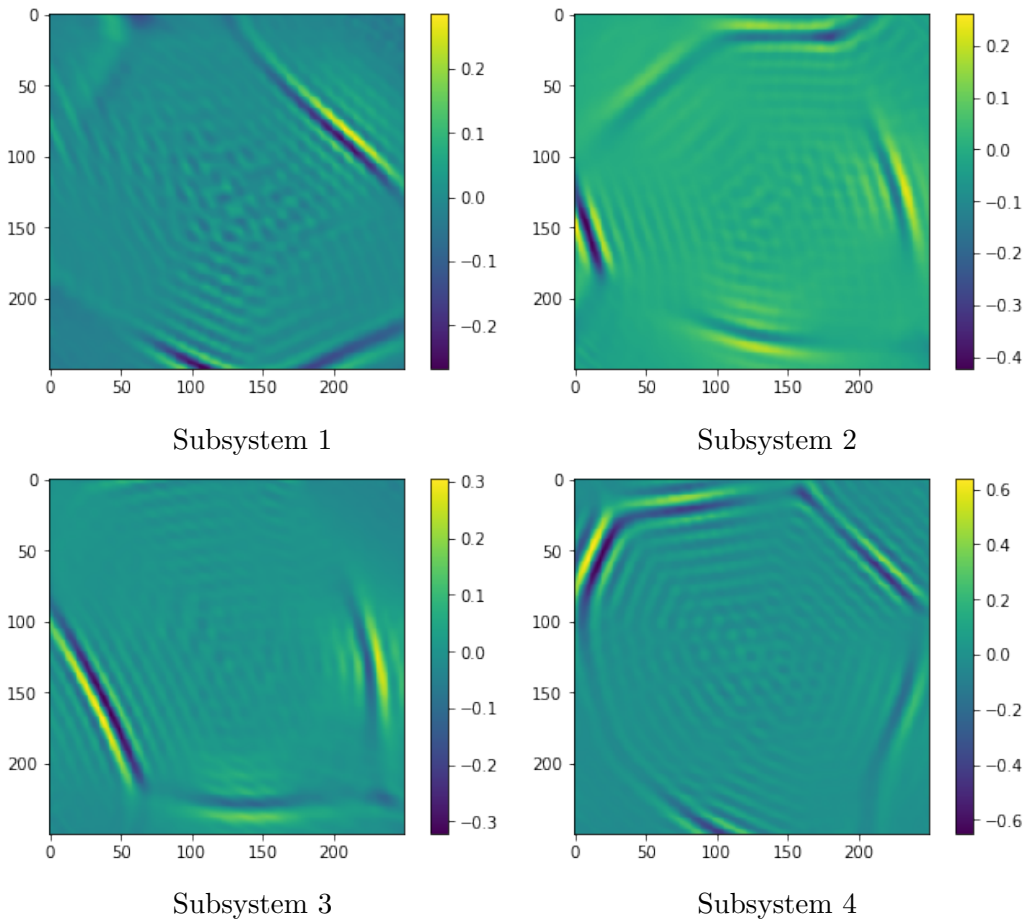

Figure 1: Differential analysis of the Embedding potential (EP) of the neutral state minus the charge state, for the four first subsystems. Calculated using PBCpy 0.2.7 Python 3 module.

The previous result for IPs of the 64 bulk water system was obtained through eQE software using PBE functional [1]. Following the same theoretical framework (PBE) once we obtained the cube file with the splined embedding potential, a Frozen Density Embedding (FDE) calculation was carried out with ADF.

As shown in figure 2, the results for IPs of isolated water, (computed considering every single molecule of the liquid to be isolated) evidence that both histograms are peaked around the average and only spreads by about 0.1 eV. If we compare both pairs of histograms the isolated and bulk ones, the latter are much broader by about 2 eV. The above agree completely with the fact that the first absorption band in the liquid, for the optical spectrum of water [19, 40–42], peaks at higher energies in comparison to the gas phase [1]. Averages IPs values for the bulk water are lower by 2.2 - 3.3 eV (eQE and ADF, respectively) in comparison with the IPs of the isolated system, it means the gas-phase. In contrast with the previously reported by Thöle et al.[1], a difference of 3.2 eV between gas-phase and liquid water, we can explain this because of the uses of open-shell for the ground-state calculations. Our results for the gas-phase are in complete agreement with experimental previously reported [33].

Furthermore, there is an underestimation of the computed IP for bulk water through ADF in comparison with eQE of 0.92 eV. We can argue the above recalling that eQE uses pseudopotential approximation that set the ion core electrons to be 'frozen' assuming they are not by definitionperturbed by physical rearrangements of the system [35], while ADF treats core orbitals from high-level all-electron atomic calculations to be frozen (but intact) for when calculating the atomic wavefunctions, consider the complete system (i.e. all the electrons)[20].

The IPs average between PBE and B3LYP functionals of the bulk liquid water present

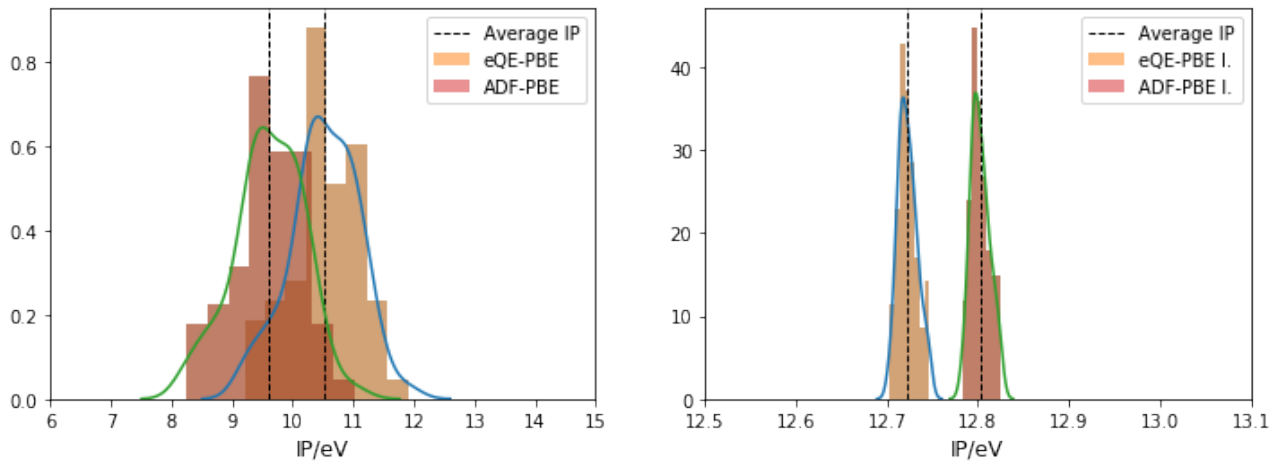

Figure 2: Comparison of the distribution of IPs of bulk liquid water between ADF[20] and eQE [14]. The area subtended by the lines sums up to 64 (ie, the number of subsystems). Left: Embedded water molecules in the bulk. Right: Isolated water molecules. Dot lines represent the average IP. The lines fitting the underlying distributions are obtained from a kernel density estimation using Seaborn's Gaussian envelopes[34]

a difference of 0.1 eV, Figure 3. The first as a generalized gradient approximation (GGA) functional for the exchange-correlation (XC) which description of the density ρ depends not only at a certain point, but also the gradient of ρ at the point, could be calling 'non-local'[16]. While the latter belongs to the hybrid approximation for the exchange-hybrid correlation functionals which defines the exchange-correlation as the inclusion of some Hartree-Fock exchange (HF) mixed with GGA exchange and correlation, plus some empirical parameters, making it certainly non-local [25]. This leads to conclude that the non-locality framework plays a crucial role when an embedding potential is used. If we compare B3LYP and SAOP (Statistical average of orbital potentials) model, the latter an asymptotical correction of the XC designed to model the KS potential with its Coulombic asymptotics for the occupied orbitals[37, 38], the difference is 0.075 eV, however, in comparison with the experimental values both underestimate the IPs by 0.4 eV. If we compare now the above XC functionals with the second-order Møller-Plasset (MP2) which is an effective Hartree-Fock ground state energy correction for the electron correlation effects, [39] we can argue that the difference of 0.4 eV among MP2 and DFT method used here is due to the not exact XC treatment of the latters.

Table 1: average IPs

	IP average (eV)
MP2	9.9941
HF	7.8250
PBE	9.6089
B3LYP	9.5147
SAOP	9.5897

The computed average IP of liquid water is summarized in Table 1 where also are displayed the results from Gas-phase and previously reported data through several level of theory.

Comparison among Liquide GW A, GW B, GW-PAW and our results.

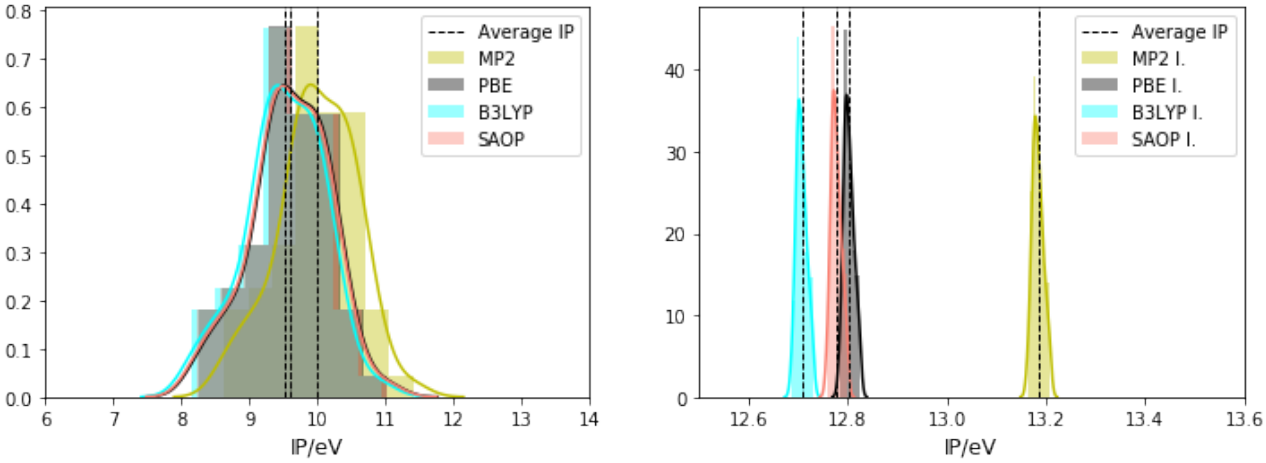

Figure 3: Distribution of IPs of bulk liquid water using MP2 and DFT methods through ADF [20]. The area subtended by the lines sums up to 64 (ie, the number of subsystems). Left: Embedded water molecules in the bulk. Right: Isolated water molecules. Dot lines represent the average IP. The lines fitting the underlying distributions are obtained from a kernel density estimation using Seaborn's Gaussian envelopes[34]

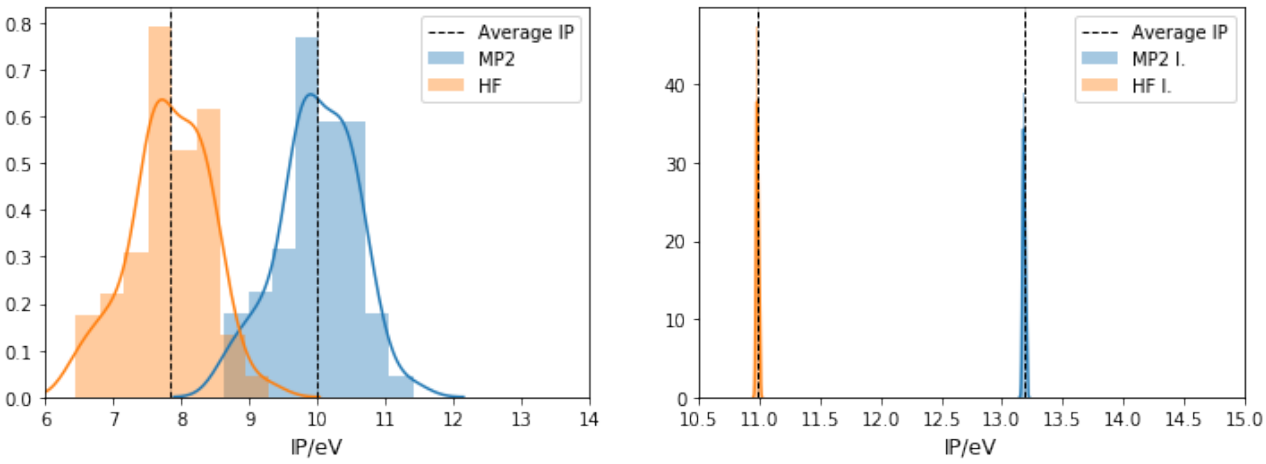

Figure 4: Distribution of IPs of bulk liquid water using MP2 and HF methods through ADF [20]. The area subtended by the lines sums up to 64 (ie, the number of subsystems). Left: Embedded water molecules in the bulk. Right: Isolated water molecules. Dot lines represent the average IP. The lines fitting the underlying distributions are obtained from a kernel density estimation using Seaborn's Gaussian envelopes[34]

5 Conclusions

References

(1) Tölle, J.; Severo Pereira Gomes, A.; Ramos, P.; Pavanello, M. *International Journal of Quantum Chemistry* **2019**, *119*, e25801.

(2) Krishtal, A.; Sinha, D.; Genova, A.; Pavanello, M. *Journal of Physics: Condensed Matter* **2015**, *27*, 183202.

(3) Bagus, P. S. *Physical Review* **1965**, *139*, A619.

(4) Waskom, M.; Botvinnik, O.; O'Kane, D.; Hobson, P.; Lukauskas, S.; Gemperline, D. C.; Augspurger, T.; Halchenko, Y.; Cole, J.; Warmenhoven, J., et al. *Zenodo, doi* **2017**, *10*.

(5) Gaiduk, A. P.; Pham, T. A.; Govoni, M.; Paesani, F.; Galli, G. *Nature communications* **2018**, *9*, 1–6.

(6) Gaiduk, A. P.; Govoni, M.; Seidel, R.; Skone, J. H.; Winter, B.; Galli, G. *Journal of the American Chemical Society* **2016**, *138*, 6912–6915.

(7) Seidel, R.; Winter, B.; Bradforth, S. E. *Annual review of physical chemistry* **2016**, *67*, 283–305.

(8) Ambrosio, F.; Miceli, G.; Pasquarello, A. *The Journal of Physical Chemistry Letters* **2017**, *8*, 2055–2059.

(9) Ziaei, V.; Bredow, T. *Journal of Physics: Condensed Matter* **2018**, *30*, 215502.

(10) Dal Corso, A. *Computational Materials Science* **2014**, *95*, 337–350.

(11) Wesolowski, T. A.; Shedge, S.; Zhou, X. *Chemical reviews* **2015**, *115*, 5891–5928.

(12) Martin, R. M.; Martin, R. M., *Electronic structure: basic theory and practical methods*; Cambridge university press: 2004.

(13) Martyna, G. J.; Tuckerman, M. E. *The Journal of chemical physics* **1999**, *110*, 2810–2821.

(14) Genova, A.; Ceresoli, D.; Krishtal, A.; Andreussi, O.; DiStasio Jr, R. A.; Pavanello, M. *International Journal of Quantum Chemistry* **2017**, *117*, e25401.

(15) Corso, A. Comput Mater Sci 95: 337, 2014.

(16) Perdew, J. P.; Burke, K.; Ernzerhof, M. *Errata:(1997) Phys Rev Lett* **1996**, *78*, 1396.

(17) Laricchia, S.; Fabiano, E.; Constantin, L.; Della Sala, F. *Journal of chemical theory and computation* **2011**, *7*, 2439–2451.

(18) Genova, A.; Ceresoli, D.; Pavanello, M. *The Journal of chemical physics* **2016**, *144*, 234105.

(19) Genova, A.; Pavanello, M., et al. *The journal of physical chemistry letters* **2017**, *8*, 5077–5083.

(20) Te Velde, G. t.; Bickelhaupt, F. M.; Baerends, E. J.; Fonseca Guerra, C.; van Gisbergen, S. J.; Snijders, J. G.; Ziegler, T. *Journal of Computational Chemistry* **2001**, *22*, 931–967.

(21) Kevorkyants, R.; Wang, X.; Close, D. M.; Pavanello, M. *The Journal of Physical Chemistry B* **2013**, *117*, 13967–13974.

(22) Pavanello, M.; Neugebauer, J. *The Journal of chemical physics* **2011**, *135*, 234103.

(23) Ramos, P.; Mankarious, M.; Pavanello, M. In *Practical Aspects of Computational Chemistry IV*; Springer: 2016, pp 103–134.

(24) Solovyeva, A.; Pavanello, M.; Neugebauer, J. *The Journal of Chemical Physics* **2012**, *136*, 05B614.

(25) Hertwig, R. H.; Koch, W. *Chemical Physics Letters* **1997**, *268*, 345–351.

(26) Yu, F. *International Journal of Quantum Chemistry* **2013**, *113*, 2355–2360.

(27) Yu, F. *The Journal of Physical Chemistry A* **2014**, *118*, 3175–3182.

(28) Kozuch, S.; Gruzman, D.; Martin, J. M. *The Journal of Physical Chemistry C* **2010**, *114*, 20801–20808.

(29) Schipper, P. R.; Gritsenko, O. V.; van Gisbergen, S. J.; Baerends, E. J. *The Journal of Chemical Physics* **2000**, *112*, 1344–1352.

(30) Gritsenko, O.; Schipper, P.; Baerends, E. *Chemical physics letters* **1999**, *302*, 199–207.

(31) Head-Gordon, M.; Pople, J. A.; Frisch, M. J. *Chemical physics letters* **1988**, *153*, 503–506.

(32) Marshall, W. *Proceedings of the Physical Society* **1961**, *78*, 113.

(33) NIST, A.-A. NIST Chemistry WebBook, SRD 69, 2015.

(34) Waskom, M.; Botvinnik, O.; O'Kane, D.; Hobson, P.; Lukauskas, S.; Gemperline, D.; Augspurger, T.; Halchenko, Y.; Cole, J.; Warmenhoven, J., et al. C., Lee, A., and Qalieh, A.: Mwaskom/Seaborn: V0. 8.0 (July 2017), 2017.

(35) Srivastava, G.; Weaire, D. *Advances in Physics* **1987**, *36*, 463–517.

(36) Saue, T.; Bast, R.; Gomes, A. S. P.; Jensen, H. J. A.; Visscher, L.; Aucar, I. A.; Di Remigio, R.; Dyall, K. G.; Eliav, E.; Fasshauer, E., et al. *The Journal of Chemical Physics* **2020**, *152*, 204104.

(37) Chong, D. P.; Gritsenko, O. V.; Baerends, E. J. *The Journal of Chemical Physics* **2002**, *116*, 1760–1772.

(38) Van Meer, R.; Gritsenko, O.; Baerends, E. *Journal of chemical theory and computation* **2014**, *10*, 4432–4441.

(39) Del Ben, M.; Hutter, J.; VandeVondele, J. *Journal of chemical theory and computation* **2012**, *8*, 4177–4188.

(40) Blase, X.; Boulanger, P.; Bruneval, F.; Fernandez-Serra, M.; Duchemin, I. *The Journal of chemical physics* **2016**, *145*, 169901.

(41) Hermann, A.; Schmidt, W.; Schwerdtfeger, P. *Physical review letters* **2008**, *100*, 207403.

(42) Hahn, P.; Schmidt, W.; Seino, K.; Preuss, M.; Bechstedt, F.; Bernholc, J. *Physical review letters* **2005**, *94*, 037404.

6 Acknowledgments